



CHORUS

This is the accepted manuscript made available via CHORUS. The article has been published as:

Evidence of the charge-density wave state in polypyrrole nanotubes

Abhisakh Sarma, Milan K. Sanyal, and Peter B. Littlewood

Phys. Rev. B **91**, 165409 — Published 13 April 2015

DOI: [10.1103/PhysRevB.91.165409](https://doi.org/10.1103/PhysRevB.91.165409)

Evidence of the charge-density wave state in polypyrrole nanotubes

Abhisakh Sarma and Milan K. Sanyal*

Saha Institute of Nuclear Physics, 1/AF Bidhannagar, Kolkata-64, India.

Peter B. Littlewood

Argonne National Laboratory, 9700 S. Cass Avenue Lemont, IL 60439, USA.

(Dated: April 1, 2015)

Abstract

We present a detailed investigation of the low-frequency dielectric and conductivity properties of conducting polymer nanowires. Our results, obtained by connecting $\sim 10^7$ nanowires in parallel, show that these polypyrrole nanowires behave like conventional charge density wave (CDW) materials, in their nonlinear and dynamic response, together with scaling of relaxation time and conductivity. The observed Arrhenius law for both these quantities gives a CDW-gap of 3.5 meV in the regime of temperature (~ 40 K) in which the CDW state survives. We find good agreement with a theory of weakly pinned CDW, screened by thermally excited carriers across the CDW gap. The identification of polymer nanowires as CDW provides us a model system to investigate charge ordering owing to electrostatic interaction, relevant to a variety of systems from dusty plasma to molecular biology.

PACS numbers: 72.15.Nj, 73.63.Fg, 77.84.Jd

I. INTRODUCTION

Spontaneous super-structures formed by electrons^{1,2} in confined materials^{3,4} are of immense importance to understand the nature of this condensate particularly in quasi-one dimensional (1D) materials¹⁻⁵ and to develop novel materials exhibiting colossal dielectric constant required for energy applications^{6,7}. The electronic charge density wave (CDW) observed in variety of crystalline materials is accompanied by a periodic lattice distortion, which can be probed by scanning tunneling microscopy or by x-ray scattering techniques⁸⁻¹⁰. The commensurability of the CDW to the underlying lattice was found to be unimportant in many cases and a recent study¹¹ has argued that the electron-electron interaction plays a primary role in CDW formation even for crystalline systems. The possibility of 1D CDW formation in jellium model (an electron gas on a positive compensating background) was predicted¹² and a possible signature of such a condensate was found in the resistive-switching transition of ultra-low doped polymer nanowires^{13,14}. Here we show that CDW condensate indeed form in polypyrrole nanowires with a gap of 3.5 meV and that transport in these nanowires behave like conventional CDW materials, except for the fact that a soliton peak become prominent at higher temperature as also observed recently in tunneling spectroscopy measurements¹⁵.

In an incommensurate CDW, collective transport is governed by the pinning of the density wave by impurities and disorder; this is coupled to quasiparticle transport produced by activation of carriers across the CDW gap. At low DC biases, the CDW is pinned and the AC response produces a dielectric loss peak associated with a broad resonance of the pinned modes. At a DC bias exceeding the threshold electric field E_{Th} for sliding, the current-voltage characteristic is nonlinear, consisting of a low-field hydrodynamic response where motion of the deformed CDW is screened by the thermally excited quasiparticles, and (switching to) a high field 'runaway' regime where the system becomes highly conducting. A characteristic of the low bias screened regime is that the complex dielectric constant $\varepsilon(\omega) = \varepsilon_1(\omega) + i\varepsilon_2(\omega)$ of a CDW shows over-damped, inhomogeneously broadened peak in ε_2 at a characteristic frequency (Ω_0) determined by relaxation time [$\Omega_0(T) = \tau_0(T)^{-1}$]. The value of the characteristic frequency changes typically from Hz to MHz as the temperature (T) increases. The observed Arrhenius law for the relaxation time $\tau_0(T)$ is characteristic of CDW state particularly because it remarkably scales with DC conductivity at low

bias condition^{1,16,17}. Here we present evidence of a CDW state in polymer nanowires by showing: nonlinear transport above a modest threshold electric field; a low frequency dielectric loss peak with a dielectric constant in the range of several thousand; and a relaxation time for the loss peak $\tau_0(T)$ whose temperature dependence scales with low bias DC conductance, both showing Arrhenius behavior with a gap of around 3.5 meV. These are classic phenomena observed in various conventional CDW materials^{16,17}.

II. EXPERIMENTAL DETAILS

The polypyrrole nanowires were synthesized chemically in polycarbonate membrane template using a two compartment cell, as described earlier¹³. Polymerization reaction occurs within the pores of the template and growth of nanowire starts from the wall, by forming first nanotubes that grows into solid nanowires. A typical transmission electron microscopy (TEM) image of these polypyrrole nanotubes is shown in Fig. 1a. In order to get the image of these nanotubes we have removed the polycarbonate membrane using Chloroform and then dropcast the nanotube solution on TEM grid. The average doping level of nanowires could be reduced drastically by reducing the diameter of these nanowires¹⁸. These polypyrrole (PPy) nanowires show characteristic of a typical quasi-one dimensional CDW system exhibiting power law behavior in current-voltage measurement, resistance switching beyond a threshold field E_{Th} ($= V_{Th}/d$, d being the thickness of the membrane), hysteresis and negative differential resistance (NDR) above resistance switching transition¹⁴. The required bias for this transition can be reduced by increasing the electron density with the help of illumination¹⁹. In Fig. 1b we have shown the current-voltage characteristics of a typical membrane having 100 nm nanowires across the bias driven switching transition at 6 K temperature. All the results presented here was obtained by connecting large number of nanowires($\sim 10^7$) in parallel with the help of gold pads deposited on both sides of the membrane^{13,14}. The graph shown in Fig. 1b corresponds to data for voltage bias measurement and upper inset showing current bias measurement data. Above a value of the applied bias V_G the pinned CDW starts to slide and above the bias V_{Th} we observe switching transition in resistance. During voltage bias measurement current

is limited by the compliance. If we then decrease the value of bias below threshold value the system remains in the low resistive state until the applied bias is lowered to V_{Re} to restore the high resistive state giving rise to a hysteresis that depends on the temperature and wire diameter. The negative differential resistance behavior is apparent in the current bias data and is shown in the upper inset of Fig. 1b. The value of V_{Th} decreases as we increase the temperature of the sample and finally the switching behavior vanishes above 65 K temperature. In Fig. 1c we have shown typical phase diagram of 100 nm nanowires to show several different zones of resistivity behavior of these nanowires as a function of temperature and bias. It is clear from the Fig. 1c that for DC bias below V_G (< 1.2 V) the resistivity follows activated behavior upto 25 K temperature and above this temperature it follows 3D variable range hopping (VRH) behavior till about 90 K. At higher temperature above VRH zone the resistivity was observed to follow a second activated behavior¹⁸. Higher bias data in this high temperature zone show rather high conductivity due to the presence of thermally generated carriers but this temperature zone (> 70 K) do not show any switching transition. Below 70 K temperature system move from VRH or activated behavior to power law behavior as the bias voltage goes above V_G (~ 1.5 V) and finally goes to highly conducting zone as the bias cross the value of V_{Th} through switching. The value of E_{Th} increases as the temperature is lowered. It should be noted that boundaries between different zones have error bars (typically 7%) due to the overlapping behavior between two different zones. Here we present results primarily from the lower left zone of the phase diagram where CDW states remains pinned below V_G .

For the electronic transport property measurements we have deposited gold electrode of 2 mm diameter on both sides of the polycarbonate membrane containing large number (10^7) of nanotubes. Using the indium pad and silver paint we have taken the contact from the gold pad. All measurements were done using quasi four probe configuration. At room temperature we have checked the linearity of the current vs voltage curve to rule out any non-ohmic behavior of the contacts. The low temperature electronic transport property were measured by loading the sample in 4 K Closed-Cycle Refrigerator having a temperature stability of 10 mK. We have used Keithley 2602A dual channel source meter, electrometer, Novo-control Alfa-A analyzer, Lakeshore 340 temperature controller with cernox temperature sensor and heater loaded in the low temperature insert for these measurements and the setup was checked properly using standard 100

$G\Omega$. All these measurements were conducted after several heat cycle of the sample and the dielectric measurements were done from 1 HZ - 10 MHz frequency range with ten points per decade. All the bias dependence measurement was done with 100 mV r.m.s. ac with the superposition of different DC voltages, starting from 0 V to 1 V in step of 100 mV.

III. RESULTS AND DISCUSSION

The dielectric constant was calculated from the measured ac conductivity using the relation

$$\varepsilon_1(\omega) = \text{Im}\sigma(\omega)/\varepsilon_0\omega \text{ and } \varepsilon_2(\omega) = (\text{Re}\sigma(\omega) - \sigma_{DC})/\varepsilon_0\omega$$

where $\varepsilon_1(\omega)$ is the real part of permittivity and $\varepsilon_2(\omega)$ is the imaginary part of permittivity. The obtained dielectric constant $\varepsilon_1(\omega)$ and $\varepsilon_2(\omega)$ at various temperatures as a function of frequency ($\omega/2\pi$) are shown in Fig. 2a and 2b respectively. It is quite clear from the presented data that the characteristic peak frequency change from 10 Hz to 1 MHz as the temperature is increased from 4 K to 45 K. We have used appropriate correction factor elaborated earlier⁷ to extract numerical values of the presented dielectric constants here. It is clear from the TEM image that the typical outer and inner diameters of these nanotubes used here are 127 nm (d_1) and 52 nm (d_2) respectively. Using these values of outer and inner diameter of nanotubes the value of the geometric correction factor⁷, given by $4/(\pi(d_1^2 - d_2^2)N)$ with pore density N (per mm^2 8×10^5) was calculated. The plotted values of $\varepsilon_1(\omega)$ and $\varepsilon_2(\omega)$ in Fig. 2a and Fig. 2b were obtained after multiplying the measured values by this average correction factor 118. It is to be noted that correction factor was not required for the presented values of $\tan\delta = \varepsilon_2(\omega)/\varepsilon_1(\omega)$ shown in Fig. 2c.

The simplest model equation of motion of a CDW starts with the collective density

$$\rho_r = \rho_c + \rho_0 \cos(Q \cdot r + \phi(r)) \quad (1)$$

and treats the CDW as a dynamical pinned elastic medium, with a dynamical phase $\phi(r, t)$. Here, Q is the natural equilibrium wave vector, ρ_c is the collective charge density transported by the CDW (i.e. all the electrons in the band) and ρ_0 is the (generally small) amplitude of the periodic density wave. If the CDW moves, the current density is then $\rho_c \dot{\phi}$, proportional to the velocity. The effects of pinning lead to an inhomogeneous $\phi(r)$, and an electric field

exerts a force $\rho_c E(r, t)$. In a uniform applied field $E(t)$, the local field on the CDW $E(r, t)$ has to be determined by coupling to the response of the free carriers, assumed to be given by their static conductivity σ and dielectric constant ε . The form of the linear response in the pinned state is that of a damped broadened oscillator. In the simplifying case of a uniformly pinned state, the response is (neglecting the CDW inertia)

$$\left[-\frac{i\omega\rho_c^2}{\sigma - i\omega\varepsilon} + v_{pin}\right]\phi = \rho_c E_0 \quad (2)$$

This reduces (at low frequencies) to a relaxational oscillator with a characteristic peak frequency

$$[\tau_0(T)]^{-1} = \Omega_0(T) = \frac{\sigma(T)v_{pin}}{\rho_c^2} \equiv \frac{4\pi\sigma(T)}{\varepsilon_0 - \varepsilon_\infty} \quad (3)$$

ε_0 and ε_∞ are low and high frequency dielectric constants^{17,20}. Generalizing to a disordered case, what is typically observed are power-law tails on the distribution²¹ i.e.

$$\varepsilon(\omega, T) = \varepsilon_\infty + \frac{\varepsilon_0 - \varepsilon_\infty}{[1 + (i\omega\tau(T))^{1-\alpha}]^\beta} \quad (4)$$

here α and β are two temperature dependent parameter. We find that $(\varepsilon_0 - \varepsilon_\infty)$ changes slowly as a function of temperature and as a result peak frequency $\Omega_0(T)$ extracted from the fitting of measured dielectric data $\varepsilon(\omega, T)$ should scale with measured DC conductivity data $\sigma(T)$, as predicted in equation 3. We now show that $\Omega_0(T)$ scales with $\sigma(T)$ for polymer nanowires as both show activated behavior.

The fitting of $\varepsilon_1(\omega)$ and $\varepsilon_2(\omega)$ data presented in Fig. 2a and 2b were carried out using a single distribution function given in equation (4). It is clear from the Fig. 3a that at low temperature the Cole-Cole plots indicate single arc over the measured frequency range and the arc is not perfectly semicircular about τ_0 . Above 10 K there is one more arc appears at high frequency side as shown clearly in the inset of Fig. 3a but the contribution of the second peak was neglected in the fitting. The $\tan \delta$ plots as a function of temperature (T) presented in Fig. 2c clearly show that, a second (small) relaxation peak appears after 6 K. This second loss peak increases but the first loss peak decreases with increase of temperature. Both these loss peaks move to high frequency as we increases the temperature. Beyond 15 K the second peak goes to higher frequency, which is outside our measurement zone. At high temperature no other arc is appearing at low frequency side and this observation rules out any contact dependence behavior.

In Table I we have shown the obtained fitted parameter α , β , τ_0 and ε_0 for all temperatures

and lines are shown in Fig. 2a and 2b. From the Table I we find β remains close to 1 indicating symmetric relaxation peak and width of this peak, given by $(1 - \alpha)\beta$, remains almost constant to a value of 0.7 with slight decrease at higher temperature as the second peak at higher frequency appears (refer Fig. 3a inset for clarity). Temperature dependence of dielectric relaxation(τ_0) and conductivity are shown in Fig. 3b and 3c respectively. From the τ_0 vs $1/T$ log plot it is clear that mean relaxation is exhibiting an activated type behavior upto 20 K, with an activation energy of 3.496 ± 0.009 meV (41.67 K). The temperature variation of DC conductivity also follow an activated type behavior in the temperature range from 4 K to 20 K with the activation energy of 3.558 ± 0.015 meV (42.4 K). The similar value of activation energy obtained from the fitting of the relaxation time and conductivity over four orders of magnitude show scaling of these properties expected in CDW state as shown in equation (3). This has been observed in conventional CDW materials,¹⁷ like blue bronze ($K_{0.3}MoO_3$), $(TaSe_4)_2I$.

As expected, the dielectric response changes strongly with modest DC bias (refer typical 15 K data and fits in Fig. 4). With the increase of DC bias the static value of dielectric constant decreases, and the peak in ϵ_2 shifts to higher frequency. By 15 K, the low frequency peak reduces at higher bias and at 1 V bias only the second peak survives. This behavior strongly suggests that at these DC voltages, the CDW has exceeded the static threshold and is creeping slowly in the hydrodynamic (screened) regime.

IV. CONCLUSIONS

It is well known that the dielectric permittivity and the threshold field in weakly pinned CDW should show opposite trend as a function of temperature and in several materials product of these two quantities remained constant²². Similar trend is observed in Fig. 4c but these two quantities change here only by a factor of 2 in the measured temperature range where the conductance and relaxation time change by 3 orders of magnitudes indicating that dynamic processes dominate in depinning of CDW as observed earlier¹⁷ in conventional materials. The existence of higher frequency loss peak has been observed earlier in conventional CDW materials and has been compared with the²² β process found in conventional glass system which relates to the dynamics of solitons pinned at impurities^{23,24}.

It is interesting to note here that unlike in conventional CDW materials²², this so-called β process in polymer nanowires appears at higher temperature (refer Fig. 2c) and the position of this high frequency peak remain almost unchanged (refer Fig. 4c) as a function of applied bias field. Whether this peak has its origin in local soliton physics¹⁵ or is a CDW plasmon¹⁶ remains unresolved by the present data.

In conclusion, the presented results of low-frequency dielectric and conductivity measurements carried out by connecting $\sim 10^7$ nanowires in parallel, clearly show that polymer nanowires are behaving like conventional charge density wave materials. The results show clear scaling of relaxation time and conductivity and the obtained CDW gap was 3.5 meV, consistent with the observed temperature zones in which CDW state survives in these nanowires. Role of electrostatic interaction in formation of ordered state is of immense importance in various fields ranging from plasma physics to biophysics²⁵. The CDW state observed in polymer nanowires provide us a simple model system to investigate condensate configurations as electron density in these nanowires can be tuned with bias and illumination.

Work at Argonne supported by DOE-BES under Contract No. DE-AC02-06CH11357.

* Electronic address: milank.sanyal@saha.ac.in

¹ P. Monceau, *Advances in Physics* **61**, 2, 325 (2012); T. Giamarchi, arXiv:cond-mat/0205099 (2002).

² E. P. Wigner, *Phys.Rev.* **46**, 1002 (1934); Y. E. Lozovik and V. I. Yudson, *JETP Lett.* **22**, 11 (1975); H. Fukuyama, P. M. Anderson, *Phys. Rev. B*, **19**, 5211 (1979); P. A. Lee and T. M. Rice, *Phys. Rev. B* **19**, 3970 (1979); H. Fukuyama and P. A. Lee, *Phys. Rev. B* **17**, 535 (1978).

³ P. Glasson, V. Dotsenko, P. Fozooni, M. J. Lea, W. Bailey, G. Papageorgiou, S. E. Anderson and A. Kristensen, *Phys. Rev. Lett.* **87**, 176802 (2001); Marc Bockrath, David H. Cobden, Jia Lu, Andrew G. Rinzler, Richard E. Smalley, Leon Balents and Paul L. McEuen, *Nature*, **397**, 598 (1999); D. G. Ress, H. Totsuji and K. Kono, *Phys. Rev. Lett.* **108**, 176801 (2012).

⁴ W. K. Hew, K. J. Thomas, M. Pepper, I. Farrer, D. Anderson, G. A. C. Jones and D. A. Ritchie, *Phys. Rev. Lett.* **102**, 056804 (2009).

⁵ N. Deng, J. D. Watson, L. P. Rokhinson, M. J. Manfra and G. A. Csáthy, *Phys. Rev. B*, **86**,

- 201301(R) (2012); C. C. Grimes and G. Adams, Phys. Rev. Lett. **42**, 795 (1979); A.N. Aleshin and Y.W. Park, in *Handbook of Conducting Polymers*, 3rd ed., edited by Terje A. Skotheim, John Reynolds (CRC Press, 26-Dec-2006).
- ⁶ P. Lunkenheimer, V. Bobnar, A. V. Pronin, A. I. Ritus, A. A. Volkov, and A. Loidl, Phys. Rev. B **66**, 052105 (2002).
- ⁷ A. Sarma and M. K. Sanyal, AIP Advances **4**, 097121 (2014).
- ⁸ C. Brun, Z.Z.Wang, and P. Monceau, Phys. Rev. B **80**,045423 (2009).
- ⁹ K. Inagaki, M. Tsubota, K. Higashiyama, K. Ichimura, S. Tanda, K. Yamamoto, N. Hanasaki, N. Ikeda, Y. Nogami, T. Ito, and H. Toyokawa, J. Phys. Soc. Jpn. **77**, 093708 (2008).
- ¹⁰ Z.Z.Wang, P. Monceau, H. Salva, C. Roucau, L. Guemas, and A. Meerschaut, Phys. Rev. B **40**, 11589 (1989).
- ¹¹ D. Mou, R. M. Konik, A. M. Tselik, I. Zaliznyak, and X. Zhou Phys Rev B **89**, 201116(R)(2014).
- ¹² H. J. Schulz, Phys. Rev. Lett **71**, 1864 (1993); M. M. Fogler, S. Teber, B.I. Shklovskii Phys. Rev. B **69**, 035413 (2004).
- ¹³ A. Rahman and M. K. Sanyal, Adv. Mater. **19**, 3956, (2007).
- ¹⁴ A. Rahman and M. K. Sanyal, Phys. Rev. B **76**, 045110 (2007).
- ¹⁵ Y. I. Latyshev, P. Monceau, S. Brazovskii, A. P. Orlov, and T. Fournier Phys Rev Lett. **95**, 266402 (2005).
- ¹⁶ P. B. Littlewood, Phys. Rev. B **33**, 6694 (1986).
- ¹⁷ R. J. Cava, P. Littlewood, R. M. Fleming, R. G. Dunn, and E. A. Rietman, Phys.Rev.B, **33**, 2439 (1986); R. J. Cava, R. M. Fleming, P. Littlewood, E. A. Rietman, L. F. Schneemeyer, R. G. Dunn, Phys. Rev. B **30**, 3228 (1984).
- ¹⁸ I. Sarkar, A. Sarma, M. K. Sanyal, S. Thie, and W. Drube, J. Appl.Phys. **114**, 163707 (2013).
- ¹⁹ A. Rahman and M. K. Sanyal, ACS Nano. **7**, 7894 (2013).
- ²⁰ G. Blumberg, P. Littlewood, A. Gozar, B. S. Dennis, N. Motoyama, H. Eisaki and S. Uchida, Science, **297**, 584 (2002).
- ²¹ S. Havriliak and S. Negami, J. Polym. Sci. C **14**, 99 (1966).
- ²² D. Starešinić, K. Biljaković, W. Brütting, K. Hosseini, P. Monceau, H. Berger, and F. Levy Phys. Rev. B **65**, 165109 (2002).
- ²³ A. Larkin, S. Brazovskii Solid State Comm. **93**, 275 (1991).

²⁴ A.F. Volkov Phys. Lett. A **182**, 433 (1993).

²⁵ Yan Levin Rep. Prog. Phys. **65**, 1577 (2002).

Figures

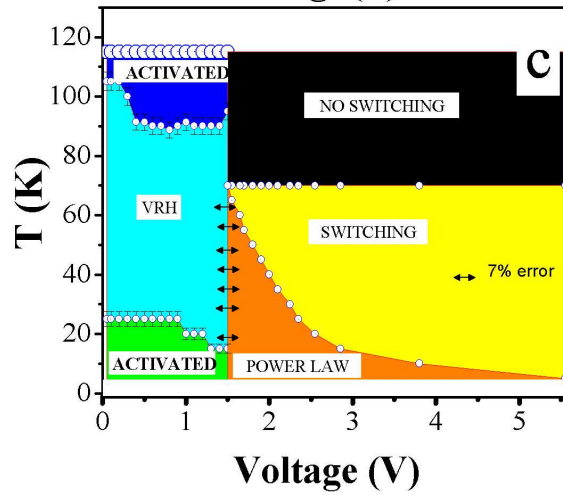
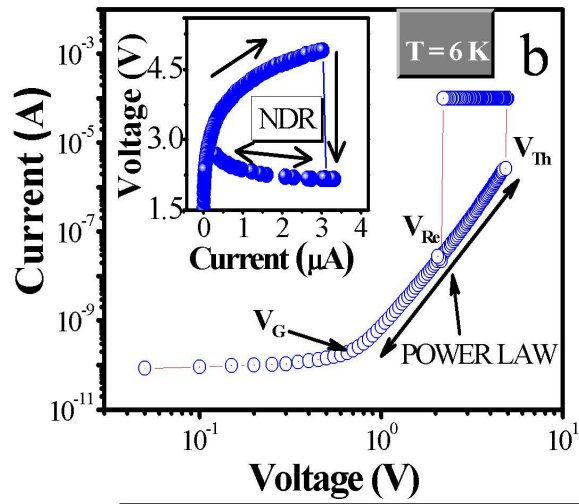
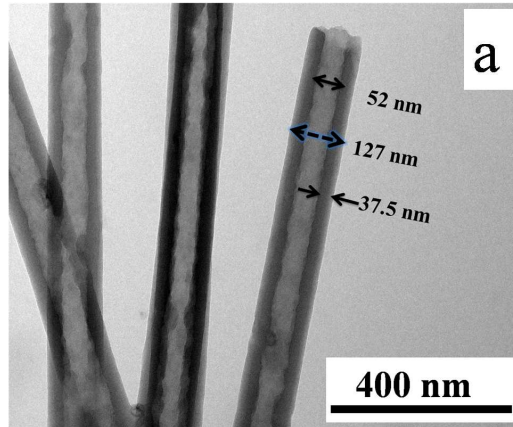


FIG. 1: (Color online) Showing (a) Current-Voltage characteristics of PPy 100 nm nanotube (solid and filled circle corresponds for voltage and current bias measurement respectively), (b) we have shown the TEM image of 100 nm nanotube, inner and outer diameter is calculated to be 52 nm and 127 nm respectively, (c) different resistivity zones of Polypyrrole nanotube of 100 nm diameter with the change of bias and temperature.

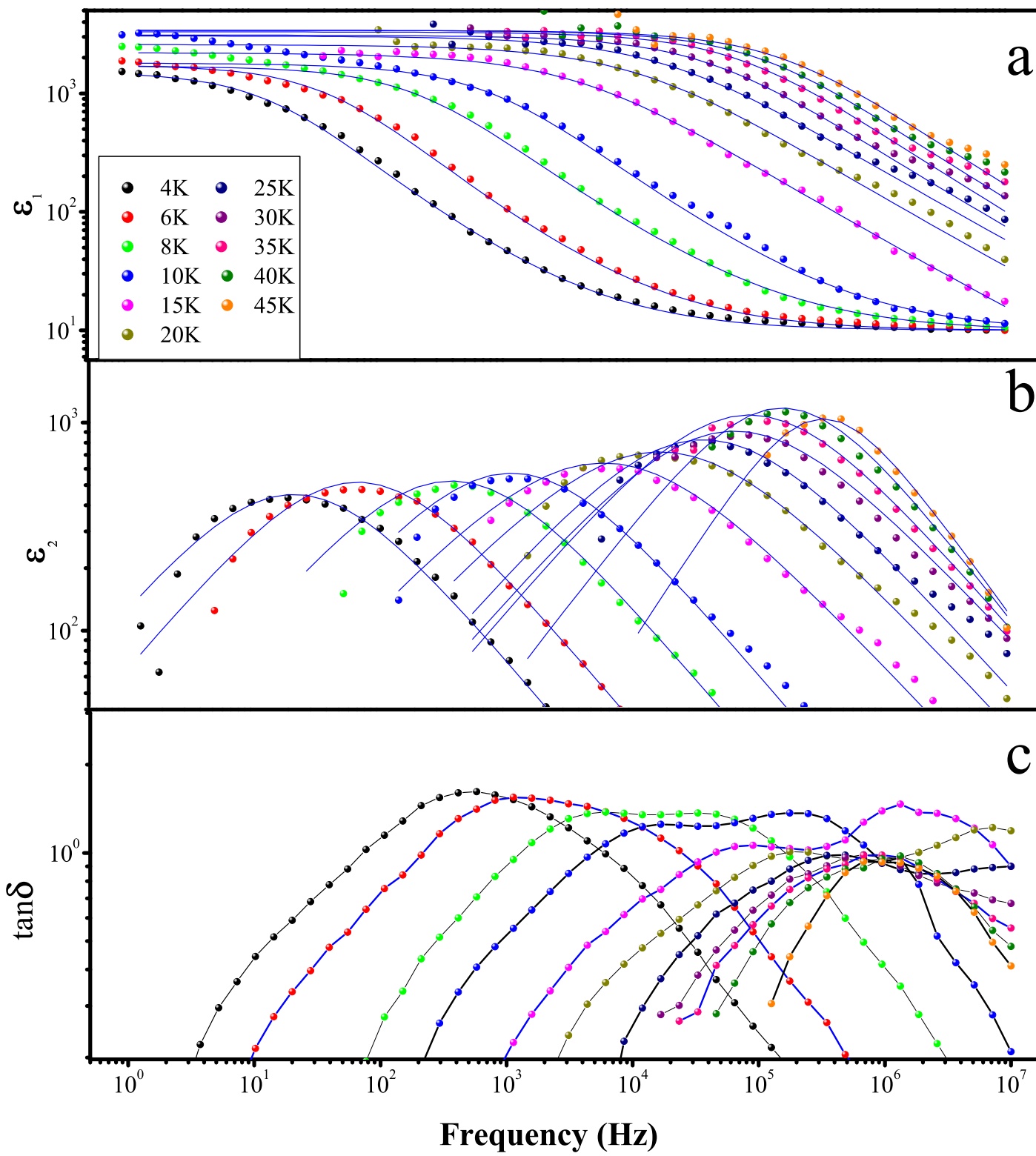


FIG. 2: (Color online) (a) Frequency dependence of real, (b) imaginary part of dielectric constant at three representative temperature is shown here. The solid lines represent the fitted data which are obtained using equation 4, (c) temperature dependence of the loss peak, after 10 K there used to arise second one peak at higher frequency which increase with the increase of temperature.

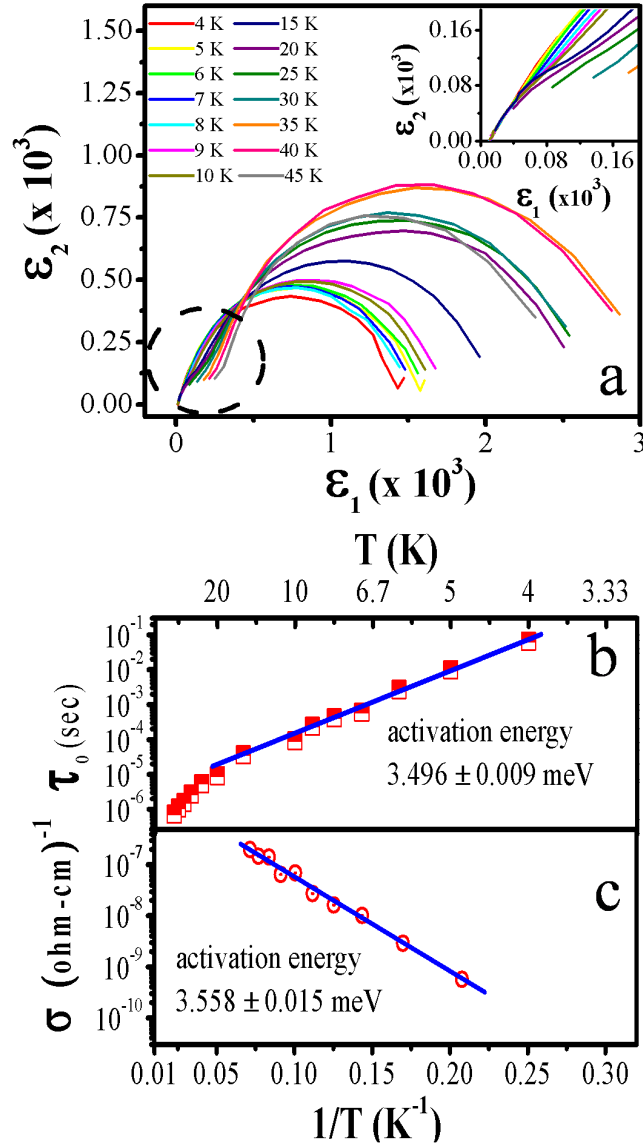


FIG. 3: (a) Temperature dependence of the Cole-Cole plot of 100 nm polypyrrole nanotube; is shown in the inset showing the magnified portion of the plot indicated by dashed circle, (b) Showing activated behavior of the mean relaxation time with temperature in the temperature range 4 K-20 K, (c) Conductivity of 100 nm Polypyrrole nanotube is following activated behavior in the temperature range 4 K-25 K.

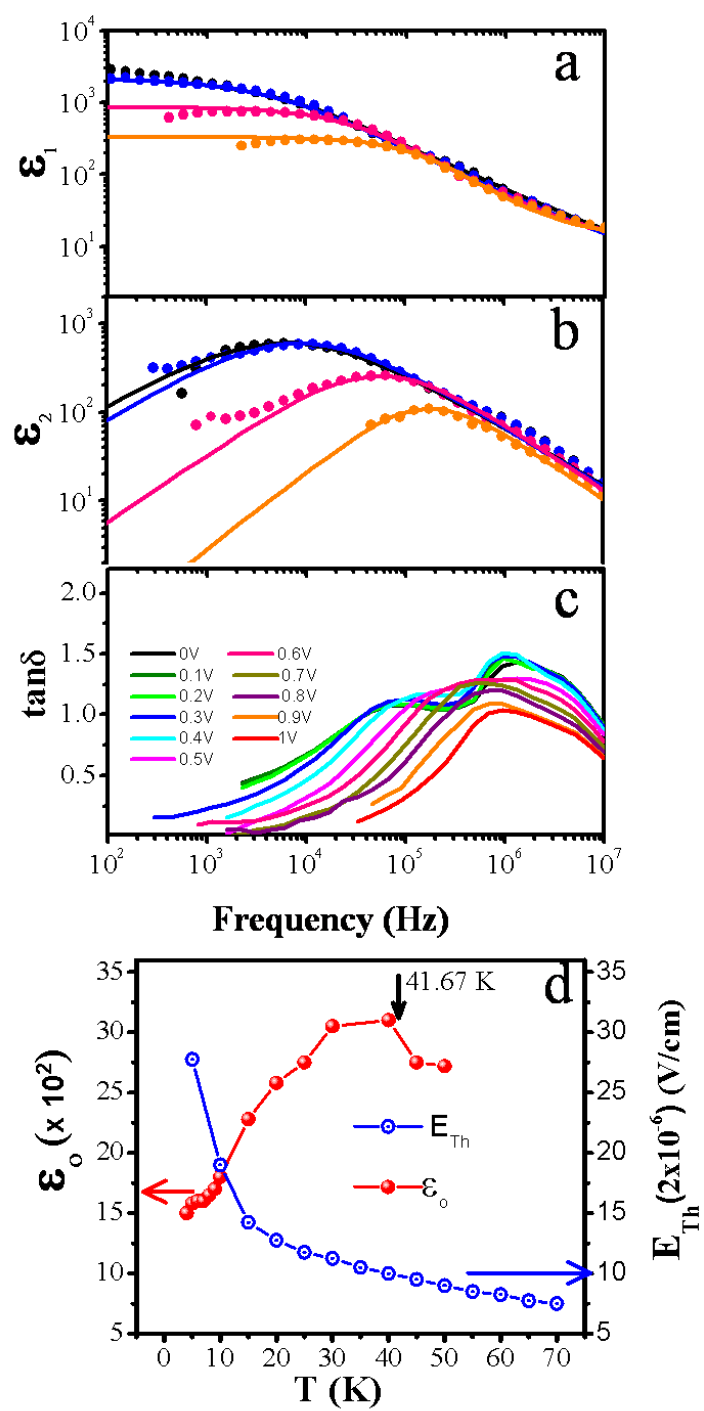


FIG. 4: Bias dependence (a) real part of dielectric constant showing the decrease of static dielectric constant with the increase of bias, (b), (c) With the increase of bias the relaxation of the low frequency peak become faster and the high frequency peak relaxation does not changes but this peak decreases with the increase of bias, (d) Temperature dependence of the static dielectric constant (ϵ_0) and the threshold field for nonlinear conductivity (E_{Th}) in Polypyrrole nanotubes.

Tables

TABLE I: The values of $\alpha, \beta, \tau_0, \epsilon_0$ obtained from the fitting of ϵ_1, ϵ_2 are shown as a function of temperature.

Temperature (K)	α	β	$\beta(\mathbf{1}-\alpha)$	τ_0 (sec)	ϵ_0
4	0.27	1	0.73	$5.21X10^{-2}$	1500
5	0.27	1	0.73	$9.86X10^{-3}$	1580
6	0.28	1	0.72	$3.1X10^{-3}$	1600
7	0.28	1	0.72	$1.1X10^{-3}$	1600
8	0.28	1	0.72	$4.93X10^{-4}$	1650
9	0.32	1	0.68	$2.38X10^{-4}$	1700
10	0.32	1	0.68	$1.387X10^{-4}$	1800
15	0.34	1	0.66	$3.043X10^{-5}$	2280
20	0.34	1	0.66	$9X10^{-6}$	2580
25	0.3	0.96	0.67	$5.4X10^{-6}$	2750
30	0.27	0.96	0.670	$2.7X10^{-6}$	3050
35	0.23	0.91	0.70	$1.53X10^{-6}$	3450
40	0.21	0.91	0.71	$1.08X10^{-6}$	2750
45	0.12	0.91	0.79	$7.2X10^{-7}$	2700